Solvation thermodynamics and heat capacity of polar and charged solutes in water

Felix Sedlmeier and Roland R. Netz

Citation: The Journal of Chemical Physics **138**, 115101 (2013); doi: 10.1063/1.4794153
View online: http://dx.doi.org/10.1063/1.4794153
View Table of Contents: http://scitation.aip.org/content/aip/journal/jcp/138/11?ver=pdfcov
Published by the AIP Publishing

Solvation thermodynamics and heat capacity of polar and charged solutes in water

Felix Sedlmeier and Roland R. Netz[a)]
Fachbereich Physik, Freie Universität Berlin, 14195 Berlin, Germany

(Received 19 November 2012; accepted 17 February 2013; published online 19 March 2013)

The solvation thermodynamics and in particular the solvation heat capacity of polar and charged solutes in water is studied using atomistic molecular dynamics simulations. As ionic solutes we consider a F^- and a Na^+ ion, as an example for a polar molecule with vanishing net charge we take a SPC/E water molecule. The partial charges of all three solutes are varied in a wide range by a scaling factor. Using a recently introduced method for the accurate determination of the solvation free energy of polar solutes, we determine the free energy, entropy, enthalpy, and heat capacity of the three different solutes as a function of temperature and partial solute charge. We find that the sum of the solvation heat capacities of the Na^+ and F^- ions is negative, in agreement with experimental observations, but our results uncover a pronounced difference in the heat capacity between positively and negatively charged groups. While the solvation heat capacity ΔC_p stays positive and even increases slightly upon charging the Na^+ ion, it decreases upon charging the F^- ion and becomes negative beyond an ion charge of $q = -0.3e$. On the other hand, the heat capacity of the overall charge-neutral polar solute derived from a SPC/E water molecule is positive for all charge scaling factors considered by us. This means that the heat capacity of a wide class of polar solutes with vanishing net charge is positive. The common ascription of negative heat capacities to polar chemical groups might arise from the neglect of non-additive interaction effects between polar and apolar groups. The reason behind this non-additivity is suggested to be related to the second solvation shell that significantly affects the solvation thermodynamics and due to its large spatial extent induces quite long-ranged interactions between solvated molecular parts and groups. © *2013 American Institute of Physics*. [http://dx.doi.org/10.1063/1.4794153]

I. INTRODUCTION

Solvation processes of molecules and molecular aggregates are ubiquitous in nature and involved in many biological phenomena. Especially the solvation of apolar hydrophobic solutes in water has received considerable attention over the last years, in part since the solvation of hydrophobic residues is generally believed to be important for the unfolding and denaturation of proteins, but certainly also because fundamental theoretical models are able to explain many of the relevant experimental features observed.[1,2] In the 1930s it was found that the solvation of small apolar solutes is characterized by a large positive heat capacity contribution ΔC_p and a negative solvation entropy ΔS at room temperature.[3,4] The negative solvation entropy means that water is more ordered around hydrophobic solutes, a finding that has received lot of attention and is considered one of the main features of hydrophobic solvation.[5–7] In fact, the solvation entropy changes its sign both when going to higher temperatures as well as when considering the solvation of larger hydrophobic solutes, which is in line with the experimental fact that the excess solvation entropy of the planar air-water interface is positive.[8] This crossover from large-scale to nanometer-scale solvation is however quite complex, reflected by the fact that the interface between water and a hydrophobic solute has a spontaneous curvature and is characterized by a negative bending rigidity.[9] As a side remark, one popular argument in favor of the dominance of the hydrophobic effect as a driving force for the folding of proteins, the observed universal entropy convergence for both protein folding and hydrophobic solvation of simple compounds,[10–12] was later questioned based on the analysis of a large set of thermodynamic protein data.[13] The spread of thermodynamic solvation data for proteins and various organic and inorganic solutes was theoretically rationalized by the fact that the solvation of hydrophobic solutes sensitively depends on specifics of the solute water interaction.[2,14] This of course does not show that the hydrophobic effect is irrelevant for protein folding, rather, it shows that drawing analogies between protein folding and solvation processes of simpler compounds is subtle.

Interestingly, the general solvation properties of hydrophilic solutes or residues are much less studied and understood than their hydrophobic counterparts. This is particularly surprising, since all biologically relevant molecules contain to a large degree hydrophilic, that is charged or neutral, polar groups. Very early, it was observed that polar compounds have a negative solvation entropy but also tend to have a much smaller or even negative heat capacity contribution.[3,4] As an extreme example, the solvation heat capacity of most salts is negative, while an unambiguous assignment of the absolute contributions of the individual ions is experimentally of course not possible.[3,15]

[a)]Electronic mail: rnetz@physik.fu-berlin.de.

Of the many thermodynamic quantities that characterize protein folding, the heat capacity has been argued to be of particular importance because of its relation with the temperature range of folding stability. To see this, we note that the isobaric heat capacity C_p measures the curvature of the Gibbs free energy $F(T, P)$ via the relation $C_p = -T\partial^2 F/\partial T^2$, where the partial temperature derivatives are taken at constant pressure P. Defining the heat capacity change associated with a solvation or a protein unfolding process ΔC_p by the difference of the heat capacity in the solvated or unfolded state minus the heat capacity in the unsolvated or folded state, a positive ΔC_p means that the free energy difference ΔF of the unfolded state minus the folded state has negative curvature. This in turn implies that if ΔF is positive and the folded state is stable at a certain temperature, the unfolded state will become stable both at high temperatures (hot denaturation, the standard scenario) as well as at low temperature (the so-called cold denaturation phenomenon, the less common but experimentally confirmed consequence of a positive ΔC_p).[16] Along the same lines, a reduced but still positive unfolding heat capacity ΔC_p would imply that the free energy of folding has a smaller curvature and thus the temperature range within which the native protein fold is stable is increased (if and only if the absolute free energy difference ΔF has the same magnitude at the temperature of maximal stability). This simple argument suggests that a reduction of the heat capacity of unfolding can be physiologically relevant for hyperthermophilic proteins that must function at elevated temperatures[16] and thus explains why physical mechanisms that would reduce the heat capacity of solvation or unfolding were at the focus of scientific activities over the last 20 yr. But we also note that this line of thought was recently questioned based on the lack of correlation between heat capacity and denaturation temperature data for a large set of thermophilic and hyperthermophilic proteins[17] and should thus be viewed as indicative and not imperative.

Clearly, the unfolding of proteins is much more complex than the solvation of model compounds, since the folding process involves conformational changes and peptide-peptide interactions that were in the early studies considered as dominant[4] and which make an unambiguous separation of the heat capacity into contributions from polar and apolar groups difficult. This is why experimental studies concentrated on oligo-peptide and model compound hydration data. As one of the most characteristic results of such studies, solvent-accessible surface models typically assign negative heat capacities to polar groups,[18,19] but it has to be kept in mind that the separation of measured heat capacity data for entire molecules into contributions from different molecular groups is highly non-trivial even for simple compounds. As one complication, the definition of polar and apolar surface areas is not unambiguous and influences the inferred group contributions.[13] But also subtle differences in chemical architecture (such as cyclic versus linear oligopeptide structures) lead to widely varying results.[20] More to the point, even in the raw data some puzzles are clearly visible: as an example, the heat capacities of molecules that only differ by COOH and $-CONH_2$ groups are very similar at all studied temperatures, while data for molecules that differ by –OH and $-NH_2$ groups without the double-bonded oxygen in the vicinity show significant deviations.[18] So one sees that even for the simplest chemical groups considered, the additivity assumption is not obeyed, which in turn suggests that interactions between neighboring chemical groups are important and lead to non-additive effects.[20,21] How and why simple additivity rules should work for the more complex problem of protein folding is therefore far from obvious.

On the theoretical side, the entropic characteristics of the solvation of polar and apolar solutes are relatively well understood.[22–26] However, extracting heat capacities directly from solvent-explicit simulations is difficult, mainly because the heat capacity being a second derivative of the solvation free energy, extremely high precision is needed, as was noted in previous simulation studies.[27] Theories were thus using various approximative methods such as the random network model,[27] angle-dependent integral equation theory,[28] or coarse-grained modeling approaches[29] and support a negative heat capacity change upon hydration of ionic and neutral polar solutes. In a recent molecular dynamics (MD) study of a wide range of polar and apolar solutes in explicit water, the radial and orientational distribution of water in the vicinity of solutes was analyzed in detail and provided insight into the distinct solvation structure around polar and apolar solutes, but a direct determination of the solvation heat capacity was not attempted in that study.[30]

It is the intent of this work to clarify the solvation thermodynamics of generic hydrophilic solutes, by direct determination of their solvation properties from atomistic molecular dynamics simulations. To that end we determine the solvation free energy ΔF as a function of the temperature for three simple solutes: a positively charged Na^+ ion, a negatively charged F^- ion, and an SPC/E water molecule as an example of a polar yet charge-neutral molecule. For all three solutes, we incrementally scale the solute charge (or partial charges in case of the water-like solute) from zero up to twice the normal charge and investigate the gradual transformation from hydrophobic to hydrophilic solvation. From the temperature dependence of the solvation free energy we obtain the solvation enthalpy ΔH, the solvation entropy ΔS, and the heat capacity change upon solvation ΔC_p. Our current study is made possible by our recently introduced method for determining the chemical potential of polar solutes with a precision of 0.01 kBT, which we have used in simulations of a stack of phospholipid membranes to fix the water chemical potential.[31] In the current paper we apply this method to the solvation of ions and polar solutes in explicit water and address two basic questions: (i) How come that polar charge-neutral solutes are typically assigned negative solvation heat capacities, while the simplest polar solute one can think of, namely a water molecule itself, has experimentally a positive solvation heat capacity?[32] (ii) How is the negative heat capacity of a neutral ion pair partitioned into the cation and the anion, in other words, is there a symmetry breaking and how is this symmetry breaking related to the water structure? In this context it is important to note that a distinct symmetry breaking of the solvation entropy between cationic and anionic solutes was found in one of the early numerical studies and associated with the asymmetric water structure around a neutral

solute.[22] Such a symmetry breaking is clearly missed in theoretical studies that use a symmetric water model[28] as well as in theories that are based on simple continuous models.[29] As our main results, we find that the charge-neutral polar solute derived from a SPC/E water molecule has a positive heat capacity that for vanishing charge agrees with what one knows for the solvation of uncharged Lennard-Jones (LJ) solutes, but also stays positive for all intermediate and higher charging factors. The tentative conclusion from these results is that negative heat capacities ascribed to polar chemical groups are artifacts arising from the neglect of the non-additive character of the heat capacity of molecules consisting of polar and apolar groups. The solvation entropy of all three different solutes exhibits a non-monotonic dependence on the charge of the solute, in line with previous results for the solvation entropy of ions,[22] which were obtained at a single temperature. We also find pronounced differences in the behavior of positively and negatively charged ions. While the heat capacity change ΔC_p decreases upon charging the F^- ion and becomes negative beyond an ion charge of $q = -0.3e$, it stays positive and even increases slightly upon charging the Na^+ ion. We further relate the non-monotonic changes in the thermodynamic observables to structural changes in the water solvation structure, in close analogy to previous findings.[30]

In Sec. II we briefly explain the computational methods employed in this work. Results are presented and discussed in Sec. III and we summarize and conclude in Sec. IV.

II. METHODS

We use molecular dynamics simulations to determine the solvation thermodynamics of a single charge-modified SPC/E water molecule, a single positively charged Na^+ and a single negatively charged F^- ion in water. In our study we vary the charge magnitude of the ionic solutes from zero to $2e$. Likewise, as an example of a generic polar yet charge-neutral solute, we scale the partial charges of the water-like solute from 0 up to twice its normal SPC/E water charge. As solvent we use the standard rigid three point charge SPC/E water model.[33] It interacts with the solutes via a Lennard-Jones potential, which is centered on the oxygen atom and electrostatically due to partial charges $q_H = 0.4238e$ and $q_O = -0.8476e$ placed on the hydrogen and oxygen atoms. The Na^+ and F^- ions are modeled as LJ spheres carrying an electric charge, the ionic LJ interaction parameters are taken from a recent force field optimization[34] (see Table I).

TABLE I. Lennard-Jones parameters for the ion-water and water-water interaction, which is of the form $V(r) = 4\epsilon[(\sigma/r)^{12} - (\sigma/r)^6]$, where r is the distance between the particles. In the SPC/E water molecule the LJ interaction is centered on the oxygen atom.

	ϵ (kJ/mol)	σ (nm)
Na^+	1.0	0.265
F^-	0.55	0.33
SPC/E	0.65	0.317

A. Solvation free energies

The solvation process for the three solutes is split up into two parts, following our previously developed methodology.[31] First, an uncharged spherical LJ particle is inserted into the solvent. The solvation free energy of this insertion, denoted as ΔF_{LJ} in the following, can be efficiently determined via the Widom particle insertion (PI) method.[35,36] In the second step the solutes are charged, the corresponding free energy change ΔF_{C} can efficiently be determined via the thermodynamic integration (TI) method. The TI method relates the free energy difference between two states I and II of a system, characterized by two potential energy functions U^{I} and U^{II}, to the averaged derivative $\langle \partial U(\lambda)/\partial\lambda \rangle$ of an intermediate potential energy $U(\lambda)$, that connects the two states by a virtual path, i.e., $U(\lambda = 0) = U^{\mathrm{I}}$ and $U(\lambda = 1) = U^{\mathrm{II}}$, where $\lambda = 0, \ldots, 2$ is a path variable. We define the states of our system by the charge $q(\lambda)$ on the solute

$$q(\lambda) = \lambda q_0, \tag{1}$$

where q_0 is the normal charge of the corresponding site. The free energy difference of charging the solute up to the charge $q(\lambda)$, $\Delta F_{\mathrm{C}}(\lambda)$ is then given by

$$\Delta F_{\mathrm{C}}(\lambda) = \int_0^{\lambda} d\lambda' \left\langle \frac{\partial U(\lambda')}{\partial \lambda'} \right\rangle_{\lambda'}, \tag{2}$$

where the average $\langle . \rangle_{\lambda'}$ has to be taken for a system interacting via $U(\lambda')$. For simulations in an isobaric-isothermal ensemble the solvation free energy contains an additional term due to the volume change,[37] which can be safely neglected in our case, since the volume change upon charging the solutes is small compared to the total system volume.

For $\lambda = 1$, we obtain the normal charge state of the solutes, that is a positive or negative unit charge for the ions and the standard partial charges for a SPC/E water molecule. It is instructive, however, to consider also solutes with charge scaling factors $\lambda < 1$, thereby illustrating the gradual transformation from a hydrophobic to a hydrophilic solute, and also to go even further and increase the range of λ up to $\lambda = 2$, corresponding to solutes with double their normal charge (i.e., divalent ions or an artificial water molecule with twice the partial charges of a normal water molecule).

The total solvation free energy for a charge scaling factor λ is then given by

$$\Delta F(\lambda) = \Delta F_{\mathrm{LJ}} + \Delta F_{\mathrm{C}}(\lambda). \tag{3}$$

We determine $\langle \partial U(\lambda)/\partial\lambda \rangle$ for 21 discrete steps, corresponding to an increment of $\Delta\lambda = 0.1$. The integral in Eq. (2) is then evaluated using the trapezoidal rule in order to avoid introducing any bias by fitting or interpolating the integrand.

For charged solutes finite size effects due to the Ewald summation can be significant. We therefore use a finite size correction term as described in Appendix A. The temperature dependence of this correction term is small, though, meaning that it is of little importance for our main results.

B. Experimental water excess chemical potential

We note that for a one-component system, and under the assumption of an ideal gas phase, the solvation free energy ΔF equals the excess chemical potential μ_{ex} in the liquid phase, defined by $\mu = \mu_{\mathrm{ex}} + \mu_{\mathrm{id}}$, where μ is the total chemical potential and μ_{id} the ideal gas chemical potential at the same number density. At gas-liquid coexistence, the particle number densities in the gas and liquid phase $\rho_{\mathrm{g,l}}$ are related via[38]

$$\rho_{\mathrm{l}} = \rho_{\mathrm{g}} e^{-\frac{\mu_{\mathrm{ex}}}{k_{\mathrm{B}}T}}, \tag{4}$$

which is a direct consequence of the homogeneity of the chemical potential in equilibrium. We use Eq. (4) to determine the water excess chemical potential from experimental data for the liquid and vapor densities along the coexistence curve[32] for comparison with our simulation results for the unmodified SPC/E water molecule for $\lambda = 1$. The difference to the simulated excess potential at constant ambient pressure at the same temperature can be estimated by $\Delta p/\rho_{\mathrm{l}}$, where Δp is the pressure difference, if we assume water to be incompressible. This correction term amounts to at most $\leq$20 J over the temperature range considered by us and can therefore safely be neglected.

C. Fitting method

In order to determine the solvation entropy, enthalpy, and the heat capacity change we fit the temperature dependence of the solvation free energy $\Delta F(\lambda)$ for each λ-value separately to a function of the form

$$\Delta F(\lambda) = a(\lambda) + b(\lambda)T - c(\lambda)T\ln(T), \tag{5}$$

from which we obtain, using $\Delta S = -\partial F/\partial T$,

$$\Delta S(\lambda) = c(\lambda)(1 + \ln(T)) - b(\lambda), \tag{6}$$

using $\Delta H = \Delta F + T\Delta S$,

$$\Delta H(\lambda) = a(\lambda) + c(\lambda)T, \tag{7}$$

and, using $\Delta C_p = \partial \Delta H/\partial T = T\partial \Delta S/\partial T = -T\partial^2 \Delta F/\partial T^2$,

$$\Delta C_p(\lambda) = c(\lambda), \tag{8}$$

i.e., by construction of our fit function for $\Delta F(\lambda)$, we assume a temperature independent heat capacity increment ΔC_p. This limitation is suggested by the fact that the absolute solvation free energies are very large in comparison with the heat capacity contribution, i.e., the curvature and therefore it is not possible to reliably extract the temperature dependence of the heat capacity change. It has been shown that even the extraction of a constant ΔC_p in such a fit can be problematic depending on the quality of the data.[39] In order to back up our fitting results for the heat capacity change, we determine ΔC_p by a second method. In this alternative approach we determine the charging enthalpy $\Delta H_{\mathrm{C}}(\lambda)$ for each temperature directly from the change in the total energy $U(\lambda)$ upon charging,

$$\Delta H_{\mathrm{C}}(\lambda) = \langle U(\lambda)\rangle - \langle U(\lambda = 0)\rangle, \tag{9}$$

and determine the charging contribution of the heat capacity change $\Delta C_{p,\mathrm{C}}$ by fitting the results for $\Delta H_{\mathrm{C}}(\lambda)$ with Eq. (7). Error estimates for $\Delta H_{\mathrm{C}}(\lambda)$ are obtained by the block averaging method, while error bars for the heat capacity change represent confidence intervals of the best fit parameters based on a confidence level of 95%. The total heat capacity change is then given by

$$\Delta C_p = \Delta C_{p,\mathrm{C}} + \Delta C_{p,\mathrm{LJ}}, \tag{10}$$

where we obtain the LJ contribution $\Delta C_{p,\mathrm{LJ}}$ from a fit of ΔF_{LJ} with Eq. (5). Note, that for the determination of the LJ contribution $\Delta C_{p,\mathrm{LJ}}$, a fit of ΔF_{LJ} according to Eq. (5) is unproblematic, since here the heat capacity contribution is much larger in comparison with the absolute values of the free energy change. A detailed discussion of the fitting methodology is found in Appendix B, where we also present results for the temperature dependence of the heat capacity of solvation.

D. Surface potential

In the context of the solvation free energy of single ions, the electrostatic surface potential of the air-water interface becomes relevant. To determine this surface potential, additional simulations in an interfacial geometry are performed. In these simulations the simulation box is only partly filled by water, which forms a homogeneous slab with two planar air/water interfaces parallel to the x/y-plane due to the periodic boundary conditions. The profile of the charge density $\rho_{\mathrm{el}}(z)$ is obtained from the atom positions by counting the partial charges into bins along the z-axis. The electric field along z, $E_z(z)$, and the electrostatic potential profile $\phi(z)$ are then obtained by integrating Poisson's equation twice, where ε_0 is the vacuum permittivity,

$$E_z(z) = \int_{-\infty}^{z} \frac{\rho_{el}(z')}{\varepsilon_0} dz', \tag{11}$$

$$\phi(z) = \int_{-\infty}^{z} E_z(z') dz'. \tag{12}$$

E. MD simulations

All molecular dynamics simulations are performed with the GROMACS simulation package,[40,41] applying periodic boundary conditions. The simulation boxes used for the thermodynamic integration contain 894 solvent water molecules and one solute molecule, resulting in a box size of roughly $3 \times 3 \times 3\ \mathrm{nm}^3$. For each λ-value the system is first equilibrated for $t = 50$ ps in an NVT (constant particle number, volume, and temperature) ensemble and subsequently for $t = 100$ ps in an NPT (constant particle number, pressure, and temperature) ensemble. All simulations are performed at ambient pressure P = 1 bar. Production runs are subsequently performed for $t = 20$ ns in the NPT ensemble. Simulations are performed for temperatures of T = 280, 300, 320, 340, 360, 380, 400, 420, and 440 K. For the higher temperatures water stays in the metastable liquid phase over the whole simulation time because of the long vapor nucleation times. Since the differences in water structure and solvation properties are minute between the coexistence and ambient pressures, our results

are also representative for water along the coexistence line. For test particle insertions a system consisting of 895 water molecules is simulated in the NPT ensemble for $t = 10$ ns at each temperature, after the same equilibration procedure as for each step of the thermodynamic integration. To determine the surface potential of the air/water interface a system containing 10 776 water molecules in a box with the size $6 \times 6 \times 15$ nm^3 is simulated, thereby forming a water slab with a thickness of roughly 9 nm in the z-direction. At each temperature it is equilibrated for $t = 100$ ps and production runs are performed for $t = 10$ ns in the NVT ensemble.

For temperature and pressure control a Berendsen weak coupling thermostat and barostat[42] with a relaxation time of $\tau = 1.0$ ps is used. All nonbonded interactions are cut off at a radius $r_c = 0.9$ nm. Long-range electrostatics are treated by the particle mesh Ewald summation technique[43,44] with tinfoil boundary conditions.

III. RESULTS AND DISCUSSION

A. Solvation thermodynamics

For clear comparison with our results for the polar solutes, we first discuss the solvation thermodynamics of hydrophobic apolar solutes. Figure 1 shows the solvation free energies of the uncharged LJ spheres, with LJ interaction parameters corresponding to a SPC/E water molecule, a Na^+ ion, and a F^- ion as a function of the temperature as well as the corresponding entropies and enthalpies obtained by fitting the free energy data as described in Sec. II. The free energy curves exhibit the typical signatures of hydrophobic solvation, i.e., pronounced curvature with a maximum around 400 K for the SPC/E and F^- LJ spheres, while the maximum for the Na^+ LJ sphere lies outside the studied temperature range. Consequently the solvation entropies and enthalpies show a positive slope. The solvation heat capacities ΔC_p obtained from the fits are 0.11, 0.06, and 0.13 kJ/(mol K) for the SPC/E, Na^+, and F^- LJ spheres, respectively, and thus are all positive, in agreement with what is known for apolar solvation.

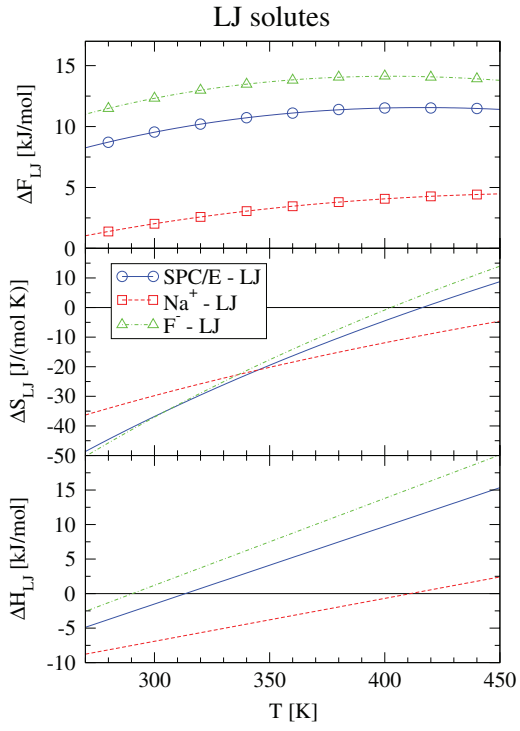

FIG. 1. From top to bottom: Solvation free energy ΔF_{LJ}, entropy ΔS_{LJ}, and enthalpy ΔH_{LJ} of LJ solutes with interaction parameters corresponding to an SPC/E water molecule without partial charges (blue circles and solid lines), a neutral version of a Na^+ ion (red squares and dashed lines), and a neutral version of a F^- ion (green triangles and dashed-dotted lines) as a function of temperature. Symbols are obtained by particle insertion, lines are obtained by fits to the data points according to Eq. (5) and Eqs. (6) and (7).

We next discuss how the solvation thermodynamics change upon the transformation from apolar to polar solutes. In Fig. 2 we show the solvation free energy $\Delta F(\lambda)$ (top row), solvation entropy $\Delta S(\lambda)$ (middle row), and solvation enthalpy $\Delta H(\lambda)$ (bottom row) for several values of the charging parameter between $\lambda = 0$ (blue lines) and 1 (red lines) as a function of temperature. The curves for $\lambda = 0$ (blue lines) correspond to the uncharged LJ solutes already shown in Fig. 1, while the curves for $\lambda = 1$ (red lines) correspond to the standard ions with unit charges and to the standard SPC/E water model, respectively.

It is seen that with increasing charge, the solvation free energies become more negative, that is, the solvation becomes more favorable. A look at the solvation enthalpies in the bottom row shows that this is mostly due to a decrease in solvation enthalpy, which overcompensates the solvation entropy which tends to decrease with increasing charge (except at low temperatures for the weakly charged solutes where the entropy shows non-monotonic behavior which will be discussed further below). So we observe that more highly charged solutes are more favorably solvated which is accompanied by a loss in entropy and thus a more ordered water solvation structure. For the water-derived polar solute, the slope of the solvation entropy decreases with increasing λ, pointing to a decrease of the heat capacity with increasing partial charge or polarity, for the F^- ion the entropy slope, and thus the heat capacity even changes its sign, while for Na^+ no dramatic change of the slope of the solvation entropy and enthalpy is observed.

To take a closer look at the variation of the thermodynamic potentials and the heat capacity with increasing charge scale parameter λ we plot $\Delta F(\lambda)$, $\Delta S(\lambda)$, $\Delta H(\lambda)$, and $\Delta C_p(\lambda)$ for all three solutes as a function of λ in Fig. 3. Note, that we here show the complete range of λ-values between 0 and 2, and thus go up to twice the normal partial charges of a SPC/E water molecule and up to two elementary charges for the ionic solutes considered by us. Different temperatures are denoted by different colors from $T = 280$ K (blue lines) up to $T = 440$ K (red lines). The top panels of Fig. 3 show the solvation free energies for each temperature. For zero charge, i.e., $\lambda = 0$, the solvation free energy is positive (as can be better seen in the insets), but with increasing λ the solvation free energies become very quickly negative. This solvation is of course much more favorable for the ions compared to the charge-modified water molecule with zero net charge, as is expected from simple continuum Born solvation models.[29] However, some subtleties require attention. As shown in the insets of Fig. 3, $\Delta F(\lambda)$ for small λ first increases slightly in

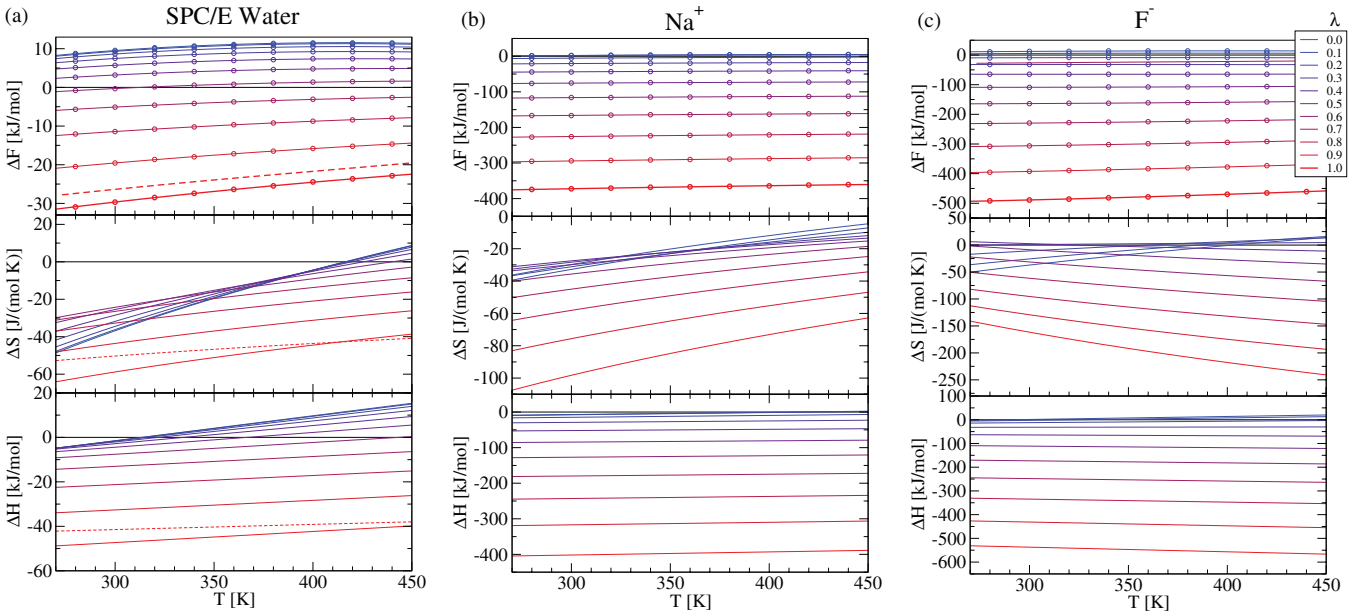

FIG. 2. From top to bottom: Solvation free energy ΔF, entropy ΔS, and enthalpy ΔH as a function of temperature for different values of the charging parameter $\lambda = 0.0$ (blue lines), 0.1, 0.2, 0.3, 0.4, 0.5, 0.6, 0.7, 0.8, 0.9, and 1.0 (red lines). Data points are simulation results, lines are fits according to Eqs. (5)–(7). From left to right: Solvation of charge-modified versions of (a) a SPC/E water molecule, (b) a Na^+ ion and (c) a F^- ion. The dashed lines in (a) show the experimental values for the excess chemical potential of water obtained via Eq. (4) from water coexistence density data[32] and the corresponding entropy and enthalpy (obtained from fits according to Eqs. (5)–(7)).

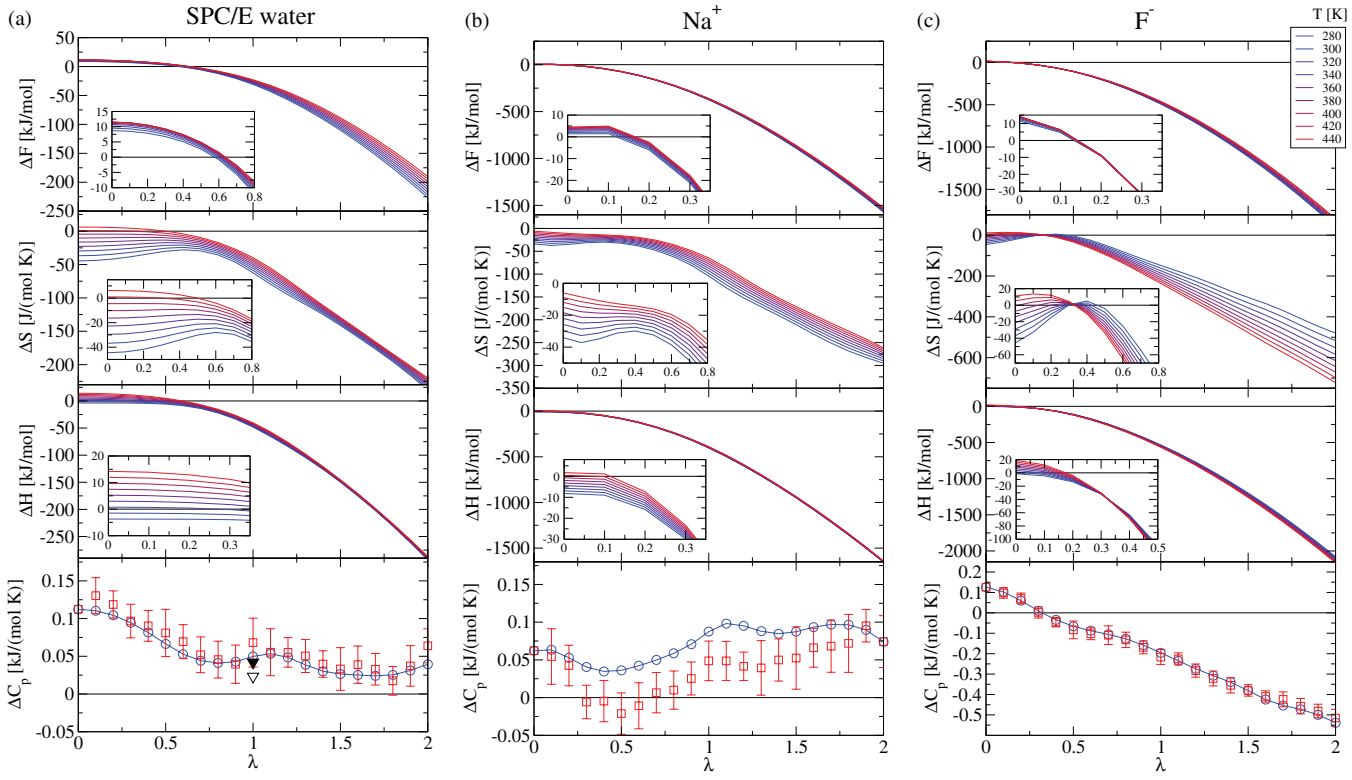

FIG. 3. From top to bottom: Solvation free energy ΔF, entropy ΔS, enthalpy ΔH, and heat capacity change ΔC_p for the solvation of charge-modified solutes in water at temperatures of $T = 280$ (blue lines), 300, 320, 340, 360, 380, 400, 420, and 440 K (red lines) as a function of the charging parameter λ. Blue circles show ΔC_p as derived from the fit according to Eq. (5) of the total solvation free energies obtained by a combination of particle insertion and thermodynamic integration, while red squares are obtained from fitting Eq. (7) to the directly obtained Coulombic solvation enthalpy and using Eq. (10). Insets show enlarged views of the small λ region. From left to right: Solvation of charge-modified versions of (a) a SPC/E water molecule, (b) a Na^+ ion, and (c) a F^- ion. Also included in (a) are the solvation heat capacities of water obtained from fitting the experimental excess chemical potential[32] either with Eq. (5) (open triangle, $\Delta C_p = 23$ J/(mol K)) or with Eq. (B2) (filled triangle, $\Delta C_p = 42$ J/(mol K)).

the case of Na^+, while it decreases monotonically with λ for F^-. The reason for this symmetry breaking is the preferential orientation of the water around an uncharged solute, which is such that on average the hydrogen atoms point slightly toward the solute and therefore the electrostatic potential inside the cavity is positive, slightly favoring a negative charge inside.[22,45] Consequently, a positively charged solute inverts the water orientation in the solvation shell, which is connected with an increase in the free energy.

This structural reorganization is reflected in the solvation entropies, which show non-monotonic behavior as a function of λ.[22] At low temperatures ΔS shows a weak maximum around $\lambda = 0.4$ for Na^+ and F^- and at $\lambda = 0.6$ for the water-derived solute (there is also a minimum around $\lambda = 0.1$ in the ΔS data for Na^+, which however is quite weak and will not be discussed). At higher temperatures, the maxima become less pronounced and even vanish completely for the water solute and Na^+ at $T = 440$ K. Overall, the solvation entropies show only a weak dependence on λ for $\lambda \lesssim 0.8$ in the case of water and Na^+ and for $\lambda \lesssim 0.5$ in the case of F^-. For higher λ values the entropy monotonically and strongly decreases for all solutes. This finding is in line with the well-documented experimental observation, that the solvation entropy of several polar solutes depends mostly on the solute volume and not so much on the degree of polarity.[23]

The lower panels in Fig. 3 show the solvation heat capacity ΔC_p as a function of λ. Blue circles connected by a solid line show results from a fit to the total solvation free energy according to Eq. (5), while red squares indicate results obtained from fitting the directly obtained charging enthalpy according to Eq. (7) as described in Sec. II. For the SPC/E water and the F^- ion both methods agree quite well within the error bars, while for the Na^+ ion there is a small but systematic difference. This is only partly due to the fact that for Na^+ the relative curvature of the solvation free energy is small. Rather, it suggests that for Na^+ the heat capacity change has a slight temperature dependence, which reflects the subtleties of solvation heat capacity determination, as will be discussed in detail in Appendix B. The λ dependence for the three solutes is markedly different. Most strikingly, for the Na^+ ion ΔC_p slightly increases with increasing λ, while for the F^- ion ΔC_p decreases strongly with increasing λ and changes its sign around $\lambda \approx 0.3$. The behavior for the water-derived solute is somewhat in between, with ΔC_p decreasing slightly while at the same time exhibiting weak oscillations, but staying strictly positive over the whole range of studied λ values. The strong symmetry breaking between positive and negative ions once again reflects that water is an asymmetric molecule and thus solvates oppositely charged solutes in a very different manner (in this respect, note the different vertical scales in the plots of the Na^+ and F^- ΔC_p data). Clearly, this symmetry breaking is difficult to observe experimentally, because there is no simple way of separating the solvation heat capacity of neutral salts into the cationic and anionic contributions. But it shows that the experimentally known negative heat capacity of common salts is caused by the anion, while the cation contributes positively. In fact, the sum of the heat capacities for the monovalent versions ($\lambda = 1$) of Na^+ ($\Delta C_p = 87$ J /(mol K)) and F^- ($\Delta C_p = -195$ J /(mol K)) yields a total of -108 J /(mol K), which is not far off the experimental value of -75 J /(mol K) for NaF.[15]

On the other hand, adding up the heat capacities of Na^+ and F^- ions with the partial charges corresponding to a standard SPC/E water molecule $q_H = 0.4238e$ and $q_O = -0.8476e$ gives a negative heat capacity, in contrast to the results obtained for water in the left column. This shows that the linear superposition of heat capacities does not work in general for neighboring chemical groups, in agreement with the experimental results for simple model compounds discussed in the Introduction.

For the standard SPC/E water heat capacity we find $\Delta C_p = 50$ J/mol K when fitting ΔF and $\Delta C_p = 70$ J/mol K when fitting the enthalpy. These simulation results are shown in the lower left panel in Fig. 3 at $\lambda = 1$ by a blue circle and a red square, respectively. Fitting the experimental excess chemical potential with Eq. (5) yields $\Delta C_p = 23$ J/mol K (open black triangle in the lower left panel in Fig. 3), while allowing for a linear temperature dependence of the heat capacity change (which is accomplished by a fit using Eq. (B2)) we obtain $\Delta C_p = 42$ J/mol K at $T = 300$ K (filled black triangle in the lower left panel in Fig. 3), in acceptable agreement with the simulation results. The comparison of the four different estimates demonstrates the subtleties of determining heat capacities from fitting free energies, which is discussed in more detail in Appendix B. Neglecting the slight temperature dependence of the water solvation heat capacity, we can obtain yet another experimental estimate, namely by taking the difference of the heat capacity of the liquid ($C_{p,l} = 76$ J/mol K) and the vapor ($C_{p,v} = 37$ J/mol K) at the boiling point at P = 1 bar,[32] which yields 39 J/mol K, again in rough agreement with the simulation fit results in the lower left panel in Fig. 3.

B. Surface potential contribution

For the solvation of neutral ion pairs from the gas phase into the aqueous phase, the contribution from the water electric surface potential cancels out. For the hypothetical process, where a single ion or a molecule with a net charge is solvated and thereby crosses the air-water interface, the surface potential contributes to the solvation free energy and has to be considered. We note that the surface potential at the interface between a solid surface and water is of similar magnitude as the air-water interfacial potential,[46] therefore the transfer free energy of net charge from the interior of a protein or a micelle is presumably influenced by similar surface potential effects. We therefore briefly discuss the temperature dependence of the surface potential of an air water interface. In Fig. 4(a) we show the surface potential profile $\phi(z)$ across an air-water interface at $T = 300$ K, the potential drop amounts to $\Delta\phi = -0.6V$. This potential is caused by a preferential orientation of the water molecules at the interface and is well-documented in literature.[47–50] If one transfers a charge across such an interface, one pays the free energy $\Delta F_{SP} = q\Delta\phi$, where q is the charge of the particle. To give an explicit example, the transfer of a monovalent cation into the water phase is favored by 0.6 eV= 58 kJ/mol, while the transfer of

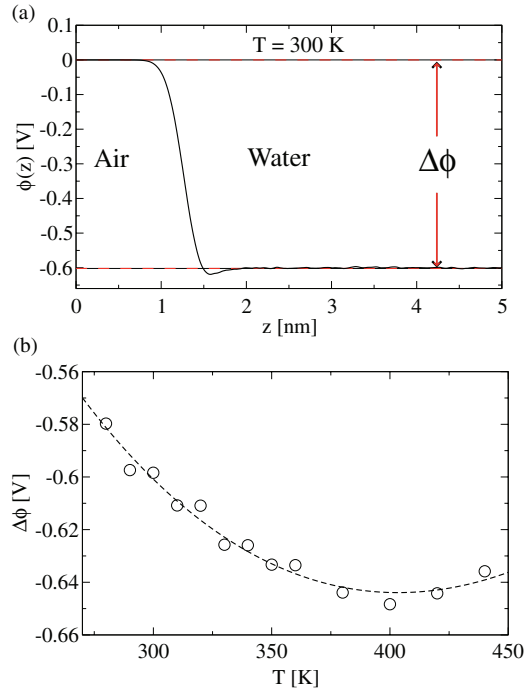

FIG. 4. (a) Surface potential profile $\phi(z)$ at an air-water interface at $T = 300$ K exhibiting a surface potential drop of $\Delta\phi = -0.6$ V. The surface potential $\phi(z)$ is set to zero in the vapor phase. (b) Surface potential drop $\Delta\phi$ at the free air/water interface as a function of the temperature (circles) and a fit according to Eq. (5) (dashed line). All data obtained from MD simulations with the SPC/E water model.

anions is disfavored by the same amount, so this effect does not correspond to a small correction but rather is very important (note that the above estimate neglects the solvation effects of ions inside the water phase and should just be considered as a rough estimate of the order of magnitude). In Fig. 4(b) we show $\Delta\phi$ at the air-water interface as a function of the temperature, which agrees qualitatively with previous simulations results[48] and with experimental estimates.[51] It is seen that $\Delta\phi$ exhibits a pronounced temperature dependence with a finite curvature. The heat capacity contribution $\Delta C_{p,\mathrm{SP}}$ from the surface potential is determined by fitting $\Delta F_{\mathrm{SP}} = q\Delta\phi$ with Eq. (5). We obtain a heat capacity contribution of $\Delta C_{p,\mathrm{SP}} = -(q/e)0.29$ kJ/(mol K). This is of the same order of magnitude as the solvation heat capacities shown in Fig. 3 and can therefore not be neglected. In fact, adding $\Delta C_{p,\mathrm{SP}}$ to the solvation ionic heat capacities would even change the signs and make the heat capacity for Na^+ negative and the heat capacity for F^- positive. The surface potential at polar surfaces depends in detail on the surface polarity and structure,[52] so it is difficult to say what the surface potential of, e.g., a protein would be, but our results presented in this section show that surface potential effects can make a sizable contribution to the solvation heat capacity of solutes with a net charge. We finally note that recent *ab initio* simulations yielded surface potential values very different from all previous classical simulations as well as experimental estimates.[53,54] It was suggested, however, that when the transfer of an ion through the air-water interface is considered, the contributions from the electric potentials at the air-water interface and around the ion itself to the solvation free energy largely cancel,[50] so we do not further discuss these complications at present.

C. Solvation structure

As has been found before, the non-monotonic dependence of the solvation entropy as a function of solute charge is related to the structure of the solvation water around the solute.[22] In this section we take a closer look at the water structure surrounding the solutes.

Figure 5 shows the radial distribution functions (RDFs) around the solutes separately for the water oxygen and hydrogen atoms $g_{X-O}(r)$ and $g_{X-H}(r)$, where $X \in \{Na^+, F^-\}$ and r is the distance between the ionic solutes and the solvent water's oxygen and hydrogen atoms, respectively, in a 2-dimensional contour plot as a function of r and λ. We first discuss the results for the Na^+ ion, shown in the top row of Fig. 5. The Na^+-oxygen RDF $g_{Na^+-O}(r)$ shows several distinctive features. With increasing λ, the peak of the first solvation shell (around $r \approx 0.28$ nm) first slightly decreases in height up to $\lambda = 0.1$ and then increases strongly up to a value of $\approx$18 at $\lambda = 2$; at the same time it slightly moves closer to the solute and becomes sharper.

In the second solvation shell more drastic restructuring occurs, in agreement with previous results.[22] The minimum around $r \approx 0.45$ nm for $\lambda = 0$ disappears for $\lambda \approx 0.5$ and for larger λ transforms into a maximum, the least structured situation for $\lambda \approx 0.5$ roughly coincides with the maximum in the solvation entropy ΔS. This suggests an intuitively appealing connection between structural disorder as described by the RDF and the solvation entropy. For larger λ values also the outer solvation shells show signs of restructuring. Complementary rearrangements are observed in the Na^+-hydrogen RDF $g_{Na^+-H}(r)$, consistent with a reversal of the preferential orientation of the hydrogen atoms from pointing toward the solute at low λ values to pointing away from the solute at higher λ values. Similar rearrangements in the second and third solvation shell can be observed.

For the negatively charged F^- ion the situation is quite different. While the F^--O RDF is qualitatively similar to the Na^+-O RDF, e.g., the first peak moves closer to the solute with increasing λ, one notes that the peaks are better defined and the distances between the peaks of the first and second solvation shells differ appreciably. The reason for this becomes clear from the F^--H RDF, which differs drastically from $g_{Na^+-H}(r)$. With increasing λ a characteristic double-peak structure develops which moves very close to the solute due to the favorable interaction of the hydrogen atom with the highly charged F^- ion. The distance between the first peaks in $g_{F^--H}(r)$ and $g_{F^--O}(r)$ is $\approx$0.1 nm, the OH distance in the SPC/E model, meaning the hydrogen atom points directly towards the F^- ion, while the other hydrogen atom points away, forming the second peak in the F^--H RDF. As for the Na^+ ion, the region between the peaks becomes depleted and the outer solvation shells become restructured with increasing λ, and the least structured situation around $\lambda \approx 0.4$ roughly coincides with the maximum in the solvation entropy ΔS. In total the solvation shell structure around the negatively charged ion

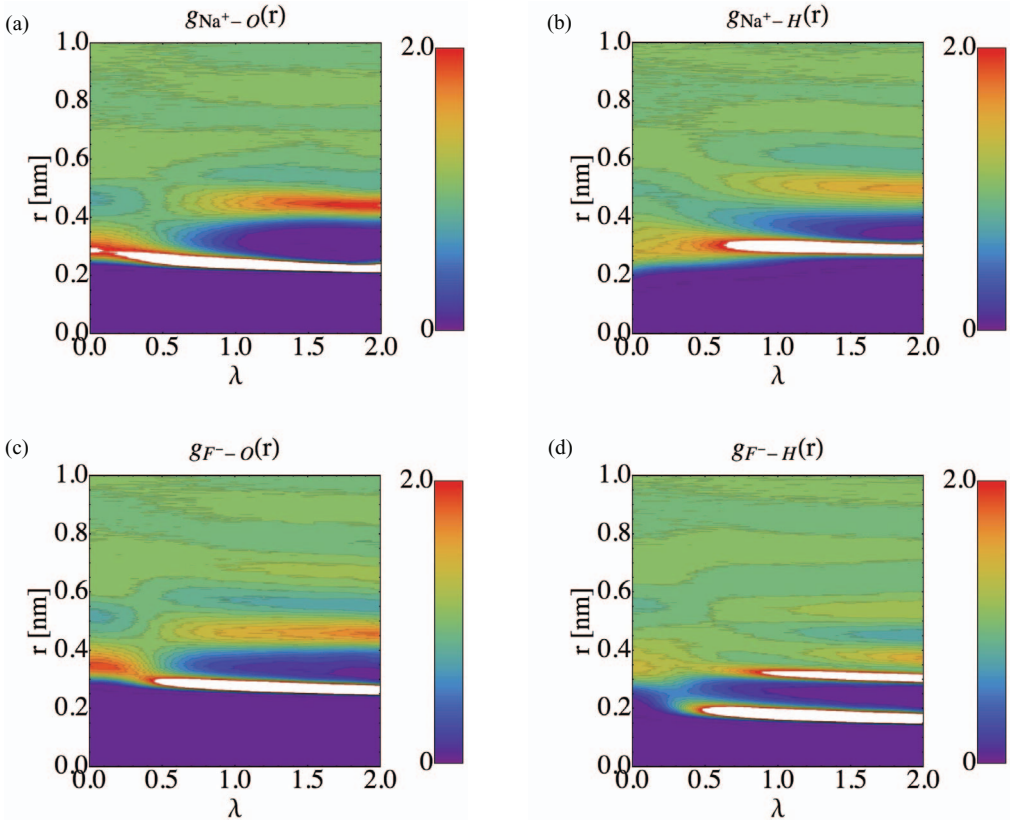

FIG. 5. (a) and (b) Pair correlation functions $g_{Na^+-O}(r)$ and $g_{Na^+-H}(r)$ between a Na^+ ion and the water oxygen and hydrogen atoms, respectively, as a function of the charging parameter λ at $T = 300$ K. (c) and (d) Same as in the top row, but for a F^- ion.

is more structured than for the positively charged ion, in line with the much more negative solvation entropy. We suggest this is the main reason for the negative solvation heat capacity of the F^- ion.

For the modified water molecule there are four partial RDFs to be considered, $g_{OM-O}(r)$, $g_{OM-H}(r)$, $g_{HM-O}(r)$, and $g_{HM-H}(r)$, where OM and HM refer to the oxygen and hydrogen atoms on the modified water molecule and O and H to the oxygen and hydrogen atoms on the normal solvating water molecules (see Fig. 6). For $\lambda < 1$ RDFs are dominated by the gradual transformation of a purely hydrophobic solute to a polar solute with hydrogen-bonding capability. A pronounced change in the RDFs around $\lambda \approx 0.6 - 0.7$ is clearly seen, indicating that this is the threshold where hydrogen bonds between the modified water molecule and the solvating water molecules change their character. Again, this value roughly coincides with the maximum in the solvation entropy in Fig. 3. For larger λ values the electrostatic attraction between OM and the solvating H atoms becomes stronger and a double peak structure in the $g_{OM-H}(r)$ RDF is seen, quite similar to the one observed for the F^- ion. Note that the double-peak structure occurs for larger λ values compared to the F^- ion, which is due to the smaller charge on the water oxygen atom ($q_0^{OM} = -0.8472$ e in the SPC/E model compared to $q_0^{F^-} = -1e$). The solvent water structure around the hydrogen atoms of the modified water molecule shows less resemblance with the one around the Na^+ ion, which can be attributed to the close proximity of the dominating oxygen atom in the solvated water molecule.

IV. SUMMARY AND CONCLUSION

Employing a recently introduced method for the accurate calculation of the solvation free energy of polar and charged solutes in water,[31] we have determined the solvation thermodynamics including the heat capacity change for three hydrophilic solutes, a positively and a negatively charged ion, and a modified water molecule as an example of a polar molecule with vanishing net charge. For all three studied solutes, we varied the charge (in case of the ions) or the partial charges (in case of the modified water molecule) proportional to a scaling factor λ in the range $0 < \lambda < 2$.

As our main result, we find that the sum of the solvation heat capacities of the Na^+ and F^- ions is negative, in agreement with experimental observations,[3,15] while the heat capacity of the charge-neutral polar solute derived from a SPC/E water molecule is positive for all charge scaling factors considered by us. The fact that the solvation heat capacity of water itself is positive is experimentally well-known and should therefore come as no surprise. On the other hand, our finding that ΔC_p of the modified SPC/E water molecule does not change much when varying λ means that the heat capacity of a large class of polar net-neutral solutes is positive. This in turn suggests that negative heat capacities, that are commonly ascribed to polar chemical groups using solvent-accessible surface models,[18,19] might arise from the neglect of the non-additive character of the heat capacity of molecules consisting of polar and apolar groups. This resonates with the well-known fact that the separation of measured heat capacity data

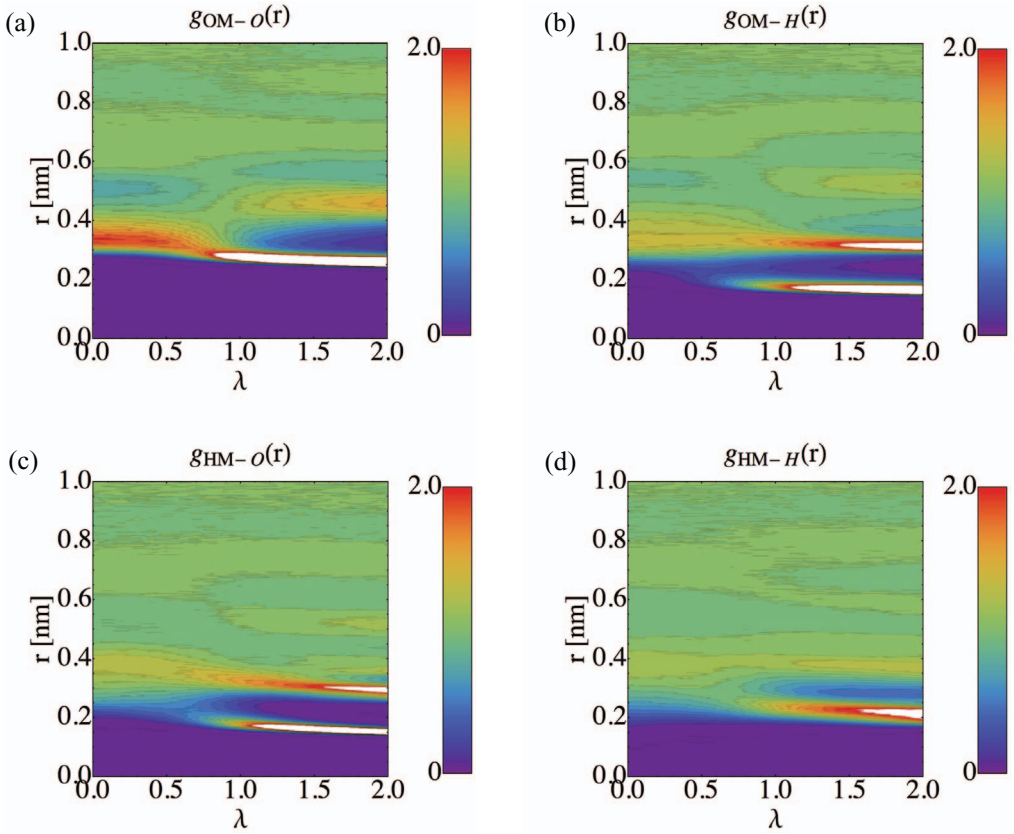

FIG. 6. (a) and (b) Pair correlation functions $g_{OM-O}(r)$ and $g_{OM-H}(r)$ between the oxygen atom of the modified water molecule OM and the oxygen and hydrogen atoms of the unmodified solvating water molecules, respectively, as a function of the charging parameter λ at $T = 300$ K. (c) and (d) Same as in the top row, but for the hydrogen atom of the modified water molecule HM.

for entire molecules into contributions from different molecular groups is highly non-trivial, as we discussed in detail in the Introduction.

The other interesting finding is the pronounced difference of the heat capacity of positively and negatively charged ions. While the heat capacity change ΔC_p decreases upon charging the F^- ion and becomes negative beyond an ion charge of $q = -0.3e$, it stays positive and even increases slightly upon charging the Na^+ ion. This symmetry breaking is closely related to the solvation water structure, which is different for solutes of opposite charge due to the intrinsic asymmetry of water molecules. While the ions chosen for our study are representative of small spherical ions, we note that F^- can to some extent be considered a non-standard ion due to its small size[55] and the pronounced charge-transfer to hydrating water molecules.[56] In future simulation work it will thus be interesting to compare the heat capacity of ions of different size.

We stress that linear superposition of heat capacities does not seem to work in general, as has been observed experimentally a long time ago.[20,21] This is illustrated by the fact that the sum of the two ionic heat capacities of $F^-$and Na^+ are strongly negative, while the heat capacity of the neutral yet polar water-derived solute stays strictly positive for all partial charges considered by us. The reason behind this non-additivity could have to do with the fact that it is the second solvation shell that significantly controls the solvation thermodynamics, which therefore leads to quite long-ranged interactions between solvated molecular parts and groups, as is corroborated by our structural analysis in Figures 5 and 6 and in line with previous results.[22]

Our results have direct consequences for the interpretation of the thermodynamic data of model compound solvation as well as protein denaturation studies. While separation of the solvation heat capacity into contributions from polar and apolar groups is ambiguous and the interpretation of some of the published data might have to be reconsidered, one probably has to look into non-additive solvation effects in more detail in the future, very close to the ideas expressed in one of the early works on protein folding thermodynamics.[4]

ACKNOWLEDGMENTS

Support from the DFG as part of the SFB 765 "Multivalency as chemical design and function principle" is gratefully acknowledged.

APPENDIX A: FINITE SIZE CORRECTIONS

In this appendix we briefly describe the finite size corrections applied to the solvation free energies as obtained from the thermodynamic integration method. Hummer *et al.*[45] have shown that ionic solvation free energies obtained using the Ewald summation method depend on the size of the simulation box. This is due to the self-interaction of the ions with

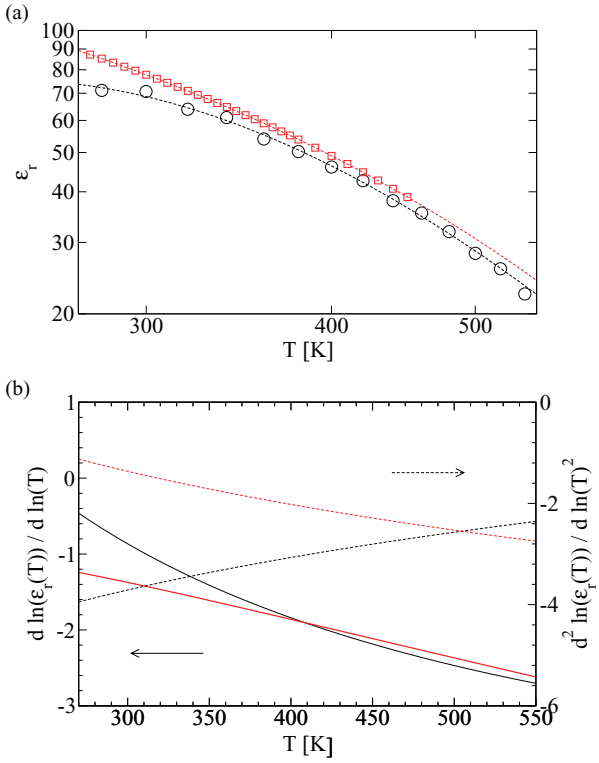

FIG. 7. (a) Relative dielectric constant ϵ_r of SPC/E water (black open circles) at a pressure of $p = 1$ bar as a function of temperature. The dashed line is a polynomial fit to the data. The red squares show the experimental results at a pressure of $p = 10$ bar.[60] (b) First logarithmic derivative of ϵ_r (solid lines, left axis) and second logarithmic derivative of ϵ_r (broken lines, right axis). Black lines denote simulation results, red lines denote experimental data.

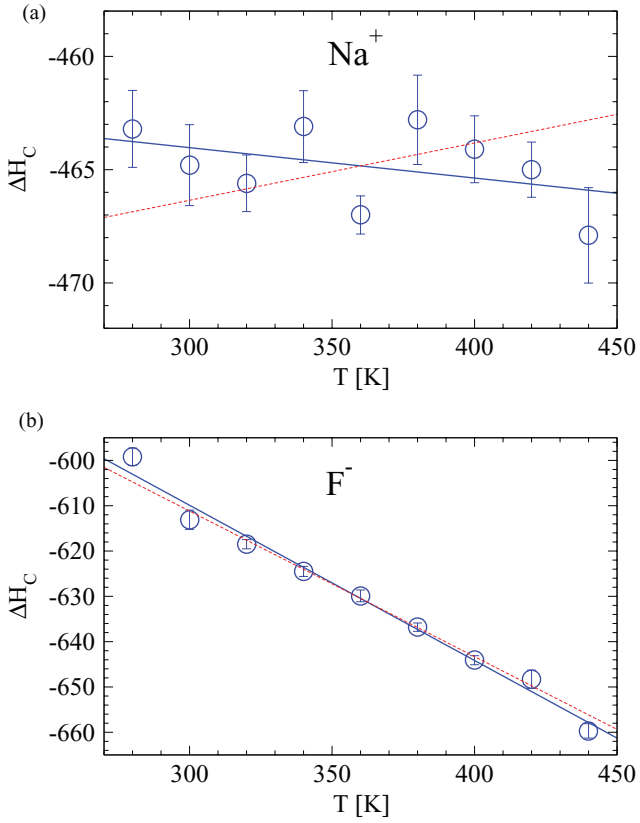

FIG. 8. Charging enthalpy ΔH_C of (a) a Na^+ ion ($\lambda = 1$) and (b) a F^- ion ($\lambda = 1$) as a function of the temperature, obtained from Eq. (9) (blue circles) including a linear fit to the data points (blue solid line) and a linear fit, where the slope is constrained to the $\Delta C_{p,C}$ value obtained from fitting Eq. (5) to the electrostatic solvation free energy (red dashed line).

their periodic images and the orientational polarization of the solvent due to the periodic images of the ions.[57,58] One can correct for these effects by calculating the free energy differences from a continuum theory,[57,58] which yields the following correction term:

$$\Delta F_{\mathrm{FS}} = \lambda^2 \frac{N_A e^2}{4\pi\epsilon_0}\left[\frac{-\zeta}{2\epsilon_r} + \left(1 - \frac{1}{\epsilon_r}\right)\left(\frac{2\pi R^2}{3L^3} - \frac{8\pi^2 R^5}{45L^6}\right)\right], \tag{A1}$$

for a particle with the charge $q(\lambda) = \lambda e$. In Eq. (A1) Avogadro's constant is denoted by $N_A = 6.022\,10^{23}$, ϵ_r is the relative dielectric constant of the solvent, and L is the box size. The Wigner potential ζ for a cubic box is given by $\zeta = -2.837\,297/L$.[45] In the MD simulations, the relative dielectric constant is determined from the variance of the fluctuations of the total dipole moment of the simulation system.[59] The result, including a cubic fit (black circles and black line), is shown as a function of temperature in Fig. 7(a), in comparison with the experimental data (red squares and red line). Figure 7(b) shows the first and second logarithmic derivatives; as can be seen, the first derivative of the simulation data (black solid line) agrees quite well with the experimental data (red solid line), while the second derivatives (black and red broken lines) differ significantly. Nevertheless, from the magnitude of the second derivative of the temperature-dependent dielectric constant, we conclude that the contribution of the correction term in Eq. (A1) to the heat capacity is negligible.

APPENDIX B: FITTING METHOD

In this appendix we discuss in detail the inaccuracies that arise when extracting heat capacities from numerical solvation data. We restate that by fitting the solvation free energy data with Eq. (5) it is implicitly assumed that the heat capacity does not depend on temperature. As an alternative way of extracting the heat capacity from the simulation data, we also used the electrostatic enthalpy ΔH_C as obtained from Eq. (9). Since ΔH_C is a small difference of two large quantities, its accuracy is quite low, as can be seen in Fig. 8. For F^-, where the temperature dependence of ΔH_C is large, the agreement between ΔH_C (blue circles and blue linear fitting curve) and a linear fit constrained to the slope corresponding to $\Delta C_{p,C}$ as obtained from fitting the electrostatic part of the solvation free energy with Eq. (5) (red broken line) is good. For Na^+ on the other hand, where the temperature dependence of ΔH_C is small, the agreement is bad.

In principle one can also include a linear temperature dependence of the solvation heat capacity

$$\Delta C_p(\lambda) = c(\lambda) + 2d(\lambda)T, \tag{B1}$$

which leads to

$$\Delta F(\lambda) = a(\lambda) + b(\lambda)T - c(\lambda)T\ln(\lambda) + d(\lambda)T^2. \tag{B2}$$

However, since the curvature of the solvation free energy is small compared to its absolute value, the introduction of

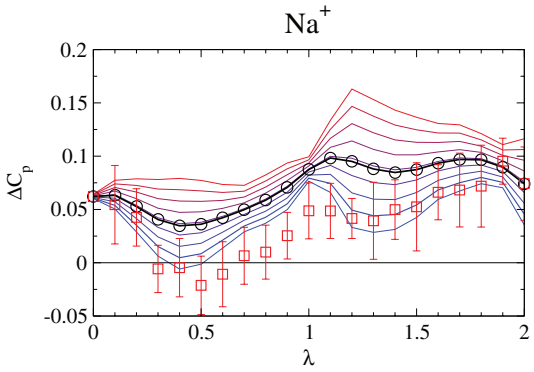

FIG. 9. Solvation heat capacity ΔC_p of a Na^+ ion as a function of the charging parameter λ. Colored lines show ΔC_p for varying temperatures of $T = 280$ (blue line), 300, 320, 340, 360, 380, 400, 420, and 440 K (red line), where a linear temperature dependence of ΔC_p has been assumed in the fit of ΔF (see Eq. (B2)). Black circles connected by a black line and red squares show ΔC_p as obtained from a fit to ΔF and ΔH, respectively, assuming a temperature independent ΔC_p and are the same data shown in the lower middle panel in Fig. 3.

higher order temperature derivatives of the solvation free energy can lead to spurious results.

In Fig. 9 we compare results for ΔC_p of a Na^+ ion from fitting the solvation free energy with the extended Eq. (B2) (colored thin lines for different temperatures) and the restricted Eq. (5) (black circles and black thick line), with the results of fitting ΔH_C to Eq. (7) (red squares). The restricted fit to the free energy (black circles) gives more or less the average of the extended fits at different temperatures (thin solid lines), while the fit to the enthalpy (red squares) follows more the results corresponding to the extended fits at lower temperatures (blue thin solid lines). We conclude that if the heat capacity exhibits a temperature dependence, using a fit expression that neglects this temperature dependence introduces a certain bias to the results, as is seen by comparing the results from using Eq. (5) to fit ΔF or Eq. (7) to fit ΔH_C. This bias is apparently not the same for both methods and therefore leads to systematic deviations between the results. In turn, the discrepancy we observe between the results obtained with the two different fitting methods points to an underlying temperature dependence of the solvation heat capacity, which unfortunately cannot be robustly resolved by our method due to the limited statistical accuracy.

[1]D. Chandler, Nature (London) **437**, 640 (2005).
[2]H. S. Ashbaugh and L. R. Pratt, Rev. Mod. Phys. **78**, 159 (2006).
[3]J. Edsall, J. Am. Chem. Soc. **57**, 1506 (1935).
[4]J. Sturtevant, Proc. Natl. Acad. Sci. U.S.A. **74**, 2236 (1977).
[5]H. Frank and M. Evans, J. Chem. Phys. **13**, 507 (1945).
[6]W. Kauzmann, Adv. Protein Chem. **14**, 1 (1959).
[7]C. Tanford, *The Hydrophobic Effect: Formation of Micelles and Biological Membranes*, 1st ed. (Wiley-Interscience, New York, 1973).
[8]K. Lum, D. Chandler, and J. D. Weeks, J. Phys. Chem. B **103**, 4570 (1999).
[9]F. Sedlmeier and R. R. Netz, J. Chem. Phys. **137**, 135102 (2012).
[10]R. L. Baldwin, Proc. Natl. Acad. Sci. U.S.A. **83**, 8069 (1986).
[11]K. P. Murphy, P. L. Privalov, and S. J. Gill, Science **247**, 559 (1990).
[12]B. Lee, Proc. Natl. Acad. Sci. U.S.A. **88**, 5154 (1991).
[13]A. D. Robertson and K. P. Murphy, Chem. Rev. **97**, 1251 (1997).
[14]F. Sedlmeier, D. Horinek, and R. R. Netz, J. Chem. Phys. **134**, 055105 (2011).
[15]M. H. Abraham and Y. Marcus, J. Chem. Soc., Faraday Trans. 1 **82**, 3255 (1986).
[16]N. Prabhu and K. A. Sharp, Annu. Rev. Phys. Chem. **56**, 521 (2005).
[17]G. Graziano, J. Therm. Anal. Calorim. **93**, 429 (2008).
[18]G. I. Makhadatze and P. L. Privalov, J. Mol. Biol. **213**, 375 (1990).
[19]V. V. Loladze, D. N. Ermolenko, and G. I. Makhadatze, Protein Sci. **10**, 1343 (2001).
[20]G. I. Makhadatze, S. J. Gill, and P. L. Privalov, Biophys. Chem. **38**, 33 (1990).
[21]S. Cabani, P. Gianni, V. Mollica, and L. Lepori, J. Solution Chem. **10**, 563 (1981).
[22]R. LyndenBell and J. Rasaiah, J. Chem. Phys. **107**, 1981 (1997).
[23]D. Ben-Amotz and R. Underwood, Acc. Chem. Res. **41**, 957 (2008).
[24]G. Graziano, Chem. Phys. Lett. **479**, 56 (2009).
[25]T. L. Beck, J. Phys. Chem. B **115**, 9776 (2011).
[26]T. L. Beck, J. Stat. Phys. **145**, 335 (2011).
[27]B. Madan and K. A. Sharp, J. Phys. Chem. **100**, 7713 (1996).
[28]M. Kinoshita and T. Yoshidome, J. Chem. Phys. **130**, 144705 (2009).
[29]H.-X. Zhou, Biophys. J. **83**, 3126 (2002).
[30]K. Gallagher and K. A. Sharp, J. Am. Chem. Soc. **125**, 9853 (2003).
[31]E. Schneck, F. Sedlmeier, and R. R. Netz, Proc. Natl. Acad. Sci. U.S.A. **109**, 14405 (2012).
[32]E. Lemmon, M. McLinden, and D. Friend, *NIST Chemistry WebBook*, NIST Standard Reference Database Number 69, edited by P. J. Linstrom and W. G. Mallard (National Institute of Standards and Technology, Gaithersburg, MD, 2010).
[33]H. J. C. Berendsen, J. R. Grigera, and T. P. Straatsma, J. Phys. Chem. **91**, 6269 (1987).
[34]D. Horinek, S. I. Mamatkulov, and R. R. Netz, J. Chem. Phys. **130**, 124507 (2009).
[35]B. Widom, J. Chem. Phys. **39**, 2808 (1963).
[36]P. Sindzingre, G. Ciccotti, C. Massobrio, and D. Frenkel, Chem. Phys. Lett. **136**, 35 (1987).
[37]M. R. Shirts, J. W. Pitera, W. C. Swope, and V. S. Pande, J. Chem. Phys. **119**, 5740 (2003).
[38]J. P. Hansen and I. R. McDonald, *Theory of Simple Liquids*, 3rd ed. (Academic, Amsterdam, 2006).
[39]J. Chaires, Biophys. Chem. **64**, 15 (1997).
[40]B. Hess, C. Kutzner, D. van der Spoel, and E. Lindahl, J. Chem. Theory Comput. **4**, 435 (2008).
[41]D. van der Spoel, E. Lindahl, B. Hess, G. Groenhof, A. E. Mark, and H. J. C. Berendsen, J. Comput. Chem. **26**, 1701 (2005).
[42]H. J. C. Berendsen, J. Postma, W. F. van Gunsteren, A. Dinola, and J. Haak, J. Chem. Phys. **81**, 3684 (1984).
[43]U. Essmann, L. Perera, M. L. Berkowitz, T. Darden, H. Lee, and L. Pedersen, J. Chem. Phys. **103**, 8577 (1995).
[44]T. Darden, D. York, and L. Pedersen, J. Chem. Phys. **98**, 10089 (1993).
[45]G. Hummer, L. Pratt, and A. Garcia, J. Phys. Chem. **100**, 1206 (1996).
[46]F. Sedlmeier, J. Janecek, C. Sendner, L. Bocquet, R. R. Netz, and D. Horinek, BioInterphases **3**, FC23 (2008).
[47]M. A. Wilson, A. Pohorille, and L. R. Pratt, J. Chem. Phys. **88**, 3281 (1988).
[48]V. P. Sokhan and D. J. Tildesley, Mol. Phys. **92**, 625 (1997).
[49]M. Paluch, Adv. Colloid Interface Sci. **84**, 27 (2000).
[50]A. Arslanargin and T. L. Beck, J. Chem. Phys. **136**, 104503 (2012).
[51]J. E. B. Randles, Phys. Chem. Liq. **7**, 107 (1977).
[52]J. Janecek and R. R. Netz, Langmuir **23**, 8417 (2007).
[53]K. Leung, J. Phys. Chem. Lett. **1**, 496 (2010).
[54]S. M. Kathmann, I.-F. W. Kuo, C. J. Mundy, and G. K. Schenter, J. Phys. Chem. B **115**, 4369 (2011).
[55]D. Horinek, A. Herz, L. Vrbka, F. Sedlmeier, S. Mamatkulov, and R. Netz, Chem. Phys. Lett. **479**, 173 (2009).
[56]W. H. Thompson and J. T. Hynes, J. Am. Chem. Soc. **122**, 6278 (2000).
[57]G. Hummer, L. Pratt, A. Garcia, B. Berne, and S. Rick, J. Phys. Chem. B **101**, 3017 (1997).
[58]G. L. Warren and S. Patel, J. Chem. Phys. **127**, 064509 (2007).
[59]M. Neumann, Mol. Phys. **50**, 841 (1983).
[60]D. Fernandez, A. Goodwin, E. Lemmon, J. Sengers, and R. Williams, J. Phys. Chem. Ref. Data **26**, 1125 (1997).